Low-Complexity Blind Synchronization and Demodulation for (Ultra-)Wideband Multi-User Ad Hoc Access

Xiliang Luo, *Student Member, IEEE*, and Georgios B. Giannakis, *Fellow, IEEE*

***Abstract*— Synchronization is a performance-critical factor in most communication systems: from classical narrowband and emerging (ultra) wideband (UWB) point-to-point links to cooperative or ad hoc networking, where access must deal with multi-user interference (MUI) and possibly severe inter-symbol interference (ISI). For universal applicability to all these scenarios, we develop a blind synchronization and demodulation scheme which relies on intermittent transmission of nonzero mean symbols. These enable MUI- and ISI-resilient timing acquisition via energy detection and low-complexity demodulation by matching to a synchronized aggregate template (SAT). The resultant SAT receiver offers distinct advantages over RAKE, has low-complexity and lends itself naturally to decision-directed enhancements. Its blind operation nicely fits the requirements of multi-user ad hoc access and its ability to handle ISI is particularly attractive for UWB communications. Analytical performance evaluation and simulations testing our novel scheme in UWB settings confirm its high potential for deployment.**

***Index Terms*— Synchronization, timing offset estimation, blind receivers, Ultra-Wideband (UWB), ad hoc multiple access, wireless sensor networks.**

I. Introduction

HAVING as goal the timing of symbol boundaries, synchronization is the first module of any coherent receiver, and thus plays a critical role in ensuring reliable communications. In narrowband (NB) transmissions over additive white Gaussian noise (AWGN) channels, timing acquisition amounts to peak-picking the correlation of the transmit-filter with its template formed at the receiver, using either maximum likelihood (ML), or lower complexity sub-optimal (e.g., early-late gate) alternatives [12]. Timing becomes more challenging with wideband (WB) transmissions over frequency-selective channels which induce intersymbol interference (ISI), especially in multiple access links where one must also deal with multiuser interference (MUI).

The challenge with ISI even in single-user wireless links arises because the receiver-template must also account for the multipath channel which is *unknown* during the synchronization phase. For this reason, data-aided algorithms relying on training symbols as well as non-data aided (blind or decision-directed) synchronizers aim at estimating timing *jointly* with the discrete-time baseband equivalent ISI channel – an approach inevitably increasing complexity. Furthermore, data-aided solutions are bandwidth consuming and interrupt information transmission for training purposes; while blind solutions require relatively long data records to reliably estimate the statistics they rely on (typically sample cyclic correlations) [22]. Synchronization challenges are magnified with ultra-wideband (UWB) transmissions where ISI effects are particularly pronounced, causing bit error rate (BER) performance to degrade severely due to mis-timing [20], and capacity to diminish when timing offset as well as channel coefficients and tap delays can not be acquired [14]. Most UWB synchronizers rely on training, some assume absence of interframe interference (IFI) and ISI [5], or, sampling rates as high as several GHz [9]. To cope with unknown channels inducing IFI (but no ISI), interesting data-aided and blind algorithms have been developed recently in [26], where UWB receivers acquire Timing via Dirty-Templates (TDT) formed from the received noisy waveform; see also [21] and [27]. Blind TDT schemes require long data records and are available only for single-user links. In multi-access scenarios, performance degrades markedly in the presence of ISI and MUI, even with data-aided TDT.

Besides multi-access UWB links envisioned for wireless indoor pico-nets [6], and potentially for low-power wireless sensor nets (WSN) outdoors [13], MUI constitutes a major performance-limiting factor when many asynchronous (NB or WB) communicators are to be synchronized e.g., at the base-station of a cellular code division multiple access (CDMA) system [19]. Most blind CDMA approaches are subspace-based and do not ensure identifiability of multipath channels and timing offsets in the presence of ISI and MUI [23]. And both blind as well as data-aided synchronizers for WB-CDMA over ISI channels are considerably complex as they need to estimate all users' channels and timing offsets, while typically they assume knowledge of the underlying (symbol-periodic or long) spreading codes [25]. Such an assumption may not be satisfied by several multi-access ad hoc protocols.

In addition to classical NB, WB or emerging UWB modems, synchronization remains the common preeminent hurdle to overcome in a number of contemporary wireless

Manuscript received September 30, 2004; revised February 10, 2005; accepted February 21, 2005. The associate editor coordinating the review of this paper and approving it for publication was G. Vitetta. This work was supported through collaborative participation in the Communications and Networks Consortium sponsored by the U. S. Army Research Laboratory under the Collaborative Technology Alliance Program, Cooperative Agreement DAAD19-01-2-0011. The U.S. Government is authorized to reproduce and distribute reprints for Government purposes notwithstanding any copyright notation thereon.

The authors are with the Department of Electrical and Computer Engineering, University of Minnesota, 200 Union Street, Minneapolis, MN 55455, USA (e-mail: {xlluo, georgios}@ece.umn.edu).

Digital Object Identifier 10.1109/TWC.2006.04640.

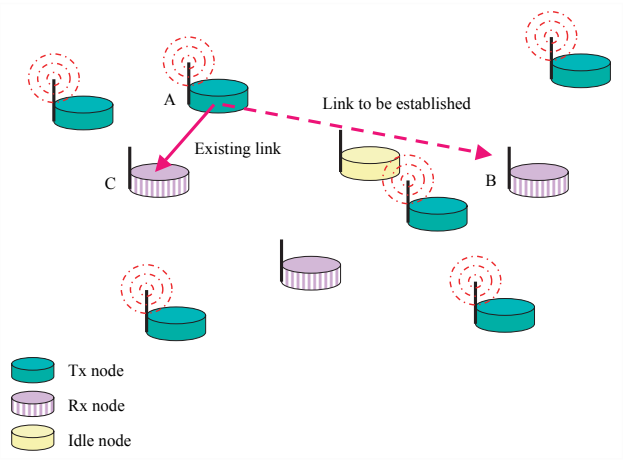

Fig. 1. A multi-access ad hoc configuration (cluster topology).

technologies including cooperative relay-communications, collaborative beamforming, distributed localization, clustering and routing [1], [8], [15], [18]. In a nutshell, there is a need for simple and preferably blind synchronizers flexible to operate with transmissions of variable bandwidth over AWGN or multipath channels, in single- or multi-user settings designed for fixed or ad hoc access.

In the present paper, we aspire to fill this need by introducing transmission protocols and low complexity receiver processors capable of ISI- and MUI-resilient timing acquisition, tracking and coherent demodulation. We will develop algorithms that can be blind and have *universal applicability* to the aforementioned scenarios, but are particularly suitable for WB or UWB multi-user ad hoc access. We will state the problem and lay out preliminary notions of our protocol in Section II. Relying on cyclostationary mean statistics and energy detection, Section III will deal with timing acquisition and recovery of what we term synchronized aggregate template (SAT) that incorporates transmit-receive filters convolved with the ISI channel. Cyclostationarity has been also utilized for blind estimation of the discrete-time equivalent channel in single-user WB [4], [28] and UWB links [24]. On top of our multi-user generalizations, even our single-user results bear objectives that are distinct from [4], [24], [28]: we aim at timing estimation and advocate recovery of the analog SAT in favor of discrete channel estimation which is costly. Moreover, we establish in Section III that a SAT-based demodulator offers advantages relative to the widely-deployed RAKE receiver. We analyze the BER of our SAT estimators and demodulators in Section IV, and develop decision-directed trackers to cope with channel variations in Section V. Corroborating simulations tailored for UWB applications are provided in Section VI, to confirm our conclusions in Section VII and testify that our novel schemes have potential for deployment because they have low-complexity and enjoy universal applicability.

II. Preliminaries and Problem Statement

Consider the ad hoc network configuration in Fig. 1, where node A is broadcasting with period T_s information bearing symbols $s(n)$ linearly modulating the transmit (spectral shaping) pulse $p_T(t)$ of duration $T_T \leq T_s$. With $\mathcal{E}$ denoting transmission energy, the transmitted waveform is:

$$u(t) = \sqrt{\mathcal{E}} \sum_n s(n) p_T(t - nT_s) \; . \tag{1}$$

This transmission can be intended for a single receiving node (point-to-point link) or even for multiple ones; and can be NB, WB or UWB. With $p_T(t) = \sum_{k=0}^{N_c-1} c_k p(t - kT_c)$, eq. (1) describes a direct-sequence CDMA transmission to (or from) a node of interest, with spreading gain N_c, symbol-periodic spreading code $\{c_k\}_{k=0}^{N_c-1}$ and chip waveform $p(t)$ of duration T_c; clearly, $T_T = T_s = N_c T_c$ here. For low-duty cycle UWB systems, $p_T(t) = \sum_{k=0}^{N_f-1} p(t - kT_f - c_k T_c)$, where $p(t)$ denotes a unit-energy pulse (a.k.a. monocycle) of duration $T_p < T_c$ (in the order of 1ns giving rise to GHz bandwidth); $T_f = N_c T_c$ is the duration of a frame comprising N_c chips; $\{c_k\}_{k=0}^{N_f-1} \in [0, N_c - 1]$ is a time hopping code[1] shifting the pulse to user-specific positions; and N_f is the number of frames (pulses) per information symbol. Here, we have $T_T = (N_f - 1)T_f + c_{N_f-1}T_c + T_p \leq T_s = N_f T_f$; see e.g., [27]. In CDMA and UWB transmissions symbols are typically BPSK with $s(n)$ taking ± 1 values equiprobably.

The multipath channel between any two nodes is allowed to be frequency-selective (and thus ISI-inducing) with impulse response $\sum_{l=0}^{L} \alpha_l \delta(t - \tau_l)$, where taps $\{\alpha_l\}_{l=0}^{L}$ and delays $\{\tau_1 < \tau_2 < \ldots < \tau_L\}$ are assumed invariant over a block of symbols (block fading model). Typically, the channel's coherence time (T_{coh}) satisfies: $T_{coh} \gg T_s$. Letting $\tau_{l,0} := \tau_l - \tau_0$, isolates the direct-path delay τ_0 which creates the timing offset between transmitter and receiver, and leads to the channel:

$$h(t) = \sum_{l=0}^{L} \alpha_l \delta(t - \tau_{l,0}). \tag{2}$$

Notice that $h(t)$ has support $[0, \tau_{L,0}]$, where the delay spread $\tau_{L,0}$ can be obtained through channel sounding. We will assume henceforth that a (preferably tight) upper bound on $\tau_{L,0}$ is available.

At a receiving node, we observe the convolution $u(t) \star h(t - \tau_0)$ in the presence of MUI $\rho(t)$ and AWGN $\eta(t)$. The latter has two-sided power spectral density $N_0/2$ and bandwidth W dictated by the ideal low-pass front-end filter's cutoff frequency. We combine transmit-, channel- and receive-filter effects in the aggregate symbol waveform $p_R(t)$ of duration $T_R := \sup\{t | p_R(t) \neq 0\}$, where $p_R(t) = \sum_{l=0}^{L} \alpha_l p_T(t - \tau_{l,0})$. Our ensuing derivations and results will rely solely on $p_R(t)$ and T_R. For this reason, $p_R(t)$ can capture more general models of the transmitter, channel and receiver modules so long as the latter represent linear time-invariant operators. Specifically, $p_R(t)$ can include distortions originating from: i) UWB transmit- and receive-antennas which act as differentiators and deform the monocycle; ii) diffuse-multipath effects which cause pulse-stretching (this time dilation can be included in T_R) [2], [6]; and iii) unknown phase errors which manifest themselves as a constant multiplicative factor

[1]Here we set $c_0 = 0$ to ensure that $\inf\{t | p_T(t) \neq 0\} = 0$. This is without loss of generality (w.l.o.g.), since we can incorporate $c_0 T_c$ into the unknown channel delay.

$\exp(j\phi_e)$. Accounting for all these effects, the waveform at the receive-filter output can be written as [c.f. (1) and (2)]

$$r(t) = \sqrt{\mathcal{E}} \sum_n s(n) p_R(t - nT_s - \tau_0) + \rho(t) + \eta(t) \ . \quad (3)$$

Given only $r(t)$, we seek a transmission protocol equipped with a synchronization pattern enabling low-complexity blind estimation of τ_0, $p_R(t)$ and detection of $s(n)$ in the presence of noise, MUI and ISI. Towards this objective, we will adopt the following operating conditions:

C1. *We choose the symbol period $T_s > \Delta\tau_{\max} - T_T$, where $\Delta\tau_{\max} \geq \max_{l\in[1,L]}(\tau_l - \tau_{l-1})$ denotes a known upper bound on successive path delay differences.*

C2. *With the delay spread $\tau_{L,0}$ (and thus T_R) known, we select an integer $M := \lceil T_R/T_s \rceil + 1$.*

C3. *During synchronization, every $M-1$ zero mean symbols $s(n)$ we transmit one nonzero mean symbol; i.e., writing $n = kM + m$ with $m \in [0, M-1]$, our symbol stream $\{s(n)\}$ taking values from a finite alphabet equiprobably, will obey: $\mathsf{E}[s(kM+m)] = \mu_0\delta(m)$ with $\mu_0 \neq 0$. Outside the synchronization interval, symbols are zero-mean throughout: $\mathsf{E}[s(n)] = 0\ \forall n$.*

C4. *MUI and AWGN in (3) are zero mean: $\mathsf{E}[\rho(t)] = \mathsf{E}[\eta(t)] = 0$.*

Condition C1 ensures that over the $[0, T_R]$ support of $p_R(t)$, intervals where $p_R(t) = 0$ are no larger than T_s, a condition whose usefulness will become clear soon. The upper bound $\Delta\tau_{\max}$ in C1 is readily available through sounding experiments, as is an upper bound on T_R. Although for clarity in exposition we rely on exact knowledge of T_R in C2, all our ensuing results carry over with an upper bound too, as we explain in Appendix A.

Notice also that in C3 we transmit a limited number of symbols (1 out M) with nonzero mean and only during the synchronization phase; otherwise, we rely on zero mean constellations that are power efficient. To maintain the same demodulator for zero-mean and nonzero mean symbols, we will effect the nonzero-mean property by minimally biasing the amplitude of certain constellation points. In CDMA or UWB settings for instance, we will use asymmetric BPSK symbols taking values $\theta, -1$ equiprobably with nonzero-mean: $\mu_0 = \mathsf{E}[s(kM)] = 0.5\theta + 0.5(-1)$, where $\theta > 1$. The same mean results if we superimpose a deterministic (training) constant $(\theta - 1)/2$ to a symmetric BPSK modulation as in [28]. However, power is wasted with superimposed training and BER performance will degrade relative to the asymmetric BPSK if we maintain the detection threshold at zero, which is desirable because the same decoder is used for both zero-mean and nonzero-mean symbols.

If the receiver can only "hear" a single transmitter broadcasting the nonzero mean synchronization pattern, then C4 is satisfied regardless of how many zero-mean interfering signals from other communicating nodes are present. This is the case with star or clustered topologies of ad hoc networks, where a single (but not always the same) node undertakes the task of synchronizing neighbors.

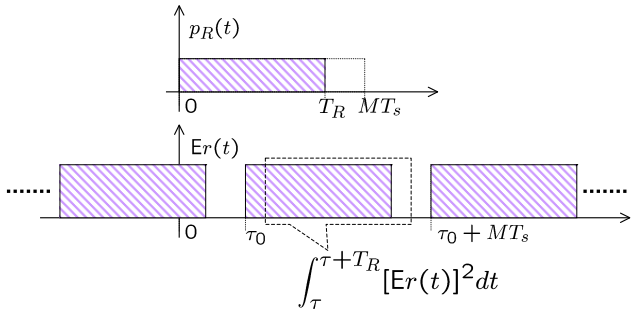

Fig. 2. Schematic illustration of the energy detector used for timing estimation.

III. Blind Synchronization and Demodulation

Under C3 and C4, the mean of the received waveform in (3) is given by:

$$\mathsf{E}r(t) = \sqrt{\mathcal{E}}\mu_0 \sum_n p_R(t - nMT_s - \tau_0) \ . \quad (4)$$

Because $\mathsf{E}r(t)$ is periodic with period MT_s, eq. (4) establishes that $r(t)$ exhibits cyclostationarity also in its mean. A period of the latter can be estimated using the mean-square sense (mss) consistent sample average across N segments of $r(t)$ each of size MT_s [3]:

$$\bar{r}(t) = \frac{1}{N} \sum_{n=0}^{N-1} r(t + nMT_s), \quad t \in [0, MT_s]. \quad (5)$$

Relying on $\mathsf{E}r(t)$ (or $\bar{r}(t)$ in practice), we will see next how we can first obtain p_R within a circular shift, and then resolve this shift to recover a synchronized aggregate template (SAT) of $p_R(t)$ that will subsequently allow us to demodulate.

A. SAT Recovery

Notice that our choice in C2 implies that over any interval of size MT_s, the mean $\mathsf{E}r(t)$ in (4) contains a circularly shifted (by τ_0) copy of $p_R(t)$ which has support of size $T_R \leq (M-1)T_s$. In fact, if τ_0 were known, then the desired SAT would be readily obtained as

$$p_R(t) = \frac{1}{\sqrt{\mathcal{E}}} \frac{1}{\mu_0} \mathsf{E}r(t + \tau_0), \quad t \in [0, T_R]. \quad (6)$$

To find τ_0, we will exploit the zero-guards of size $MT_s - T_R \geq T_s$ present in each period of $\mathsf{E}r(t)$; see Figure 2. To this end, let τ be a candidate shift (timing offset) which w.l.o.g. we confine to $[0, MT_s)$ as per (4). With $\tau \in [0, MT_s)$, consider the objective function: $J(\tau) := \int_0^{T_R} [\mathsf{E}r(t+\tau)]^2 dt$, which for the correct timing $\tau = \tau_0$ extracts the whole energy of $p_R(t)$; i.e., $J(\tau_0) = \mathcal{E}\mu_0^2 E_R$, where $E_R := \int_0^{T_R} p_R^2(t) dt$ denotes the SAT energy. We will show that τ_0 is the *unique* maximum of $J(\tau)$. For $\tau \in [0, MT_s)$, the integration in $J(\tau)$ over the interval of size T_R will span at most two periods of $\mathsf{E}r(t)$ (recall that each period has size $MT_s > T_R$). Specifically, if $\tau > \tau_0$ only the periods corresponding to $n = 0, 1$ in (4) will appear[2], yielding $J(\tau) = \mathcal{E}\mu_0^2[\int_0^{T_R} p_R^2(t + \tau - \tau_0)dt + \int_0^{T_R} p_R^2(t - MT_s + \tau - \tau_0)dt]$. Recalling that $p_R(t) = 0$

[2]Likewise, if $\tau < \tau_0$ then $n = -1, 0$ and being completely analogous to those with $\tau > \tau_0$ the subsequent steps of the proof for $\tau < \tau_0$ are omitted.

for $t \notin [0, T_R]$, we obtain $J(\tau) = \mathcal{E}\mu_0^2[\int_{\tau-\tau_0}^{T_R} p_R^2(t)dt + \int_0^{\tau-\tau_0-(MT_s-T_R)} p_R^2(t)dt]$, which can be re-written as:

$$J(\tau) = J(\tau_0) - \int_{\tau-\tau_0-(MT_s-T_R)}^{\tau-\tau_0} \mathcal{E}\mu_0^2 p_R^2(t)dt. \quad (7)$$

Because of C1, the integral in the right hand side is lower bounded for $\tau - \tau_0 > 0$ by the positive quantity $\int_{\tau-\tau_0-T_s}^{\tau-\tau_0} p_R^2(t)dt > 0$. This implies that for $\tau > \tau_0$ (and likewise for $\tau < \tau_0$), we have $J(\tau) < J(\tau_0)\ \forall \tau \neq \tau_0$, and therefore:

$$\tau_0 = \arg \max_{\tau\in[0,MT_s)} J(\tau)\ , \quad J(\tau) := \int_0^{T_R} [\mathsf{E}r(t+\tau)]^2 dt\ . \quad (8)$$

Using (5) to replace ensemble- with sample-mean estimates in (8) and (6), establishes the main result of this subsection on blind synchronization and SAT recovery, which we summarize next.

Proposition 1: *Under C1-C4, the timing offset τ_0 and the SAT $p_R(t)$ can be estimated blindly in the presence of ISI and MUI using*

$$\begin{aligned} \hat{\tau}_0 &= \arg \max_{\tau\in[0,MT_s)} \int_0^{T_R} \bar{r}^2((t+\tau)_{\text{mod } MT_s})dt\ , \\ \hat{p}_R(t) &= \frac{1}{\sqrt{\mathcal{E}}}\frac{1}{\mu_0}\bar{r}(t+\hat{\tau}_0), \quad t \in [0, T_R]\ , \end{aligned} \quad (9)$$

where the $(\text{mod } MT_s)$ operation is used because $\bar{r}(t)$ in (5) is estimated over a period of size MT_s whereas the integration in (9) needs its periodic extension.

With regards to implementation, $\bar{r}(t)$ can be computed either digitally or in analog form. Analog approaches avoid the possibly high sampling rates needed in the UWB regime, but implementing the analog delay required to shift successive $r(t)$ segments by MT_s in (5) can be challenging. Nonetheless, chips implementing analog delays from 20-1,000ns are available [29]. On the other hand, when sampling at $1-2$GHz can be afforded, it is possible to store $\bar{r}(t)$ digitally, which facilitates the maximization required to find $\hat{\tau}_0$. As far as the maximization algorithm itself, we certainly need to evaluate the objective function in (9) over a finite grid of equispaced (by say T_δ) candidate offset values to obtain: $\hat{\tau}_0 = \hat{k}T_\delta$, where $\hat{k} = \arg\max_{k\in[0,\lfloor MT_s/T_\delta\rfloor]} \int_0^{T_R} \bar{r}^2((t+kT_\delta)_{\text{mod } MT_s})dt$. Notice that timing acquisition is possible at any desirable resolution (T_δ), and is only constrained by the affordable complexity: i) coarse timing with low complexity, e.g., by picking the maximum over MN_f candidate offsets $\tau_k = kT_f$, where integer $k \in [0, MN_f)$; ii) fine timing with higher complexity at the chip resolution with $\tau_i = iT_c$, $i \in [0, MN_fN_c)$; or iii) adaptive timing estimation (tracking) with voltage-controlled clock (VCC) circuits.

It is worthwhile to stress the universal applicability of Proposition 1 to NB, WB and UWB regimes, in the presence or absence of ISI and/or MUI, with fixed or ad hoc access. Only readily available upper bounds on channel parameters are required, for low-complexity blind estimation based on sample averaging and energy detection. In the ISI-free case, we have $T_R \leq T_s$ and $M = 2$ suffices. Notice that no available approach can acquire timing of UWB transmissions in the generic setting allowed herein. Neither information bearing transmission must be interrupted for training nor transmit-filters, channels or spreading codes need to be known, so long as they remain invariant[3] while averaging in (5) is performed.

Relying on fractional sampling, cyclostationarity in the sampled correlation has long been exploited to blindly estimate the *discrete-time* equivalent aggregate channel that also includes the receive-filter; see e.g., [4] and references therein. However, these schemes are more complex and require redundancy at the transmitter (e.g., excess bandwidth). Lower complexity discrete-time alternatives relying on the cyclostationarity in the mean are offered in [28] and [24]. The latter effects the nonzero mean via pulse position modulation in a UWB context, while the former utilizes superimposed training symbols (that reduce power efficiency) for blind estimation of discrete-time single-user channels. Apart from its generic applicability to multi-access settings, and contrary to all existing approaches, our estimators in (9) bypass channel estimation and instead acquire the timing offset and the *continuous-time* SAT – a step leading to improved demodulation as will see in the next subsection. A remark is due before that.

Remark 1: Although training is to be avoided in ad hoc access, if available in a point-to-point link, we can take M odd and alternate our $M-1$ zero-mean ± 1 symbols per synchronization period so that their mean is deterministically zero. For a given accuracy, this will require a smaller N in the sample average (5). Lowering N is also possible using a decision-directed version of Proposition 1. After SAT recovery and demodulation, the $M-1$ zero-mean estimated symbols inducing ISI can be annihilated from $r(t)$ and an improved SAT estimated can be obtained, as we will see in Section V. But also outside the synchronization phase, decision-directed SAT recovery and demodulation is possible as we will detail in Section V.

B. SAT-Based Demodulation

With the continuous-time SAT available, we can built either an analog or a digital demodulator. For the latter, one has to first sample $\hat{p}_R(t)$ and $r(t)$ and proceed as in any other digital receiver. However, to maintain the full energy in $p_R(t)$, we recommend demodulation using a SAT-based correlator. Specifically, we form the decision statistic: $d(k) = \int_0^{T_R} \hat{p}_R(t)r(t+\hat{\tau}_0+kT_s)dt$ using the $\hat{p}_R(t)$ and $\hat{\tau}_0$ obtained as in (9). Substituting $r(t)$ from (3), we can re-write $d(k)$ as

$$\begin{aligned} d(k) &= \sqrt{\mathcal{E}}\phi_{\hat{p}_Rp_R}(0;\tilde{\tau}_0)s(k) + \eta(k;\tilde{\tau}_0) + \rho(k;\tilde{\tau}_0) \\ &+ \sqrt{\mathcal{E}} \sum_{n=-2(M-1),n\neq 0}^{2(M-1)} \phi_{\hat{p}_Rp_R}(n;\tilde{\tau}_0)s(k+n), \end{aligned} \quad (10)$$

where $\tilde{\tau}_0 := \tau_0 - \hat{\tau}_0$, $\phi_{\hat{p}_Rp_R}(n;\tilde{\tau}_0) := \int_0^{T_R} \hat{p}_R(t)p_R(t-nT_s-\tilde{\tau}_0)dt$, $\eta(k;\tilde{\tau}_0) := \int_0^{T_R} \hat{p}_R(t)\eta(t+kT_s+\hat{\tau}_0)dt$, and likewise for $\rho(k;\tilde{\tau}_0)$.

Based on (10), Viterbi's Algorithm (VA), sphere decoding, or, linear equalization can be invoked depending on the application-specific tradeoff between BER and affordable

[3]This explains why we only included symbol-periodic CDMA spreading in our unifying transmission model. Long aperiodic spreading codes do not apply since they change from symbol to symbol.

complexity. In UWB receivers, where (sub-)chip rate sampling is prohibitive, VA applied to $d(k)$ is the only ML optimal (in the absence of MUI) UWB receiver based on symbol-rate samples.

To further reduce complexity, one can absorb the ISI and MUI plus AWGN terms in (10) into a single colored noise term and proceed with a low-complexity (albeit sub-optimal) slicer. In CDMA and UWB single- or multi-user access with binary symbol transmissions this amounts to demodulating symbols with the sign detector:

$$\hat{s}(k) = \mathsf{sign}\left[\int_0^{T_R} \hat{p}_R(t) r(t + \hat{\tau}_0 + kT_s) dt\right] . \quad (11)$$

Summarizing our result in this section, we have:

Proposition 2: *Both during and after the synchronization phase, ML optimal, linear equalization and low-complexity matched filter options are available for demodulating $s(k)$ from the decision statistic in (10) that is based on the MUI- and ISI-resilient SAT and timing estimated blindly under C1-C4 as in (9).*

Besides its applicability to a wide range of scenarios discussed after Proposition 1, the SAT-based matched filter demodulator deserves special attention. This is because it offers a receiver with robustness, lower complexity and better performance than the RAKE receiver which is the typical choice when ISI is present. With our notation, the RAKE with maximum ratio combining (MRC) processes $r(t)$ with the filter $\sum_{l=0}^{L_r} \hat{\alpha}_l p_T(t - \hat{\tau}_l)$, where $L_r + 1$ (typically $\ll L$) denotes the number of fingers and $\{\hat{\alpha}_l, \hat{\tau}_l\}_{l=0}^{L_r}$ are estimated to approximate the dominant taps and delays of the unknown multipath channel. SAT has lower complexity than RAKE for two reasons: i) it replaces costly estimation of $\{\hat{\alpha}_l, \hat{\tau}_l\}_{l=0}^{L_r}$ with a simple recovery of $\hat{\tau}_0$ and $\hat{p}_R(t)$; and ii) instead of L_r correlators each with template $p_T(t)$ of duration T_s, (11) needs just a single correlation with $\hat{p}_R(t)$ of duration T_R. Its improved performance stems from the fact that SAT collects the full energy (and thus multipath diversity) of the channel, whereas RAKE can only approximate that of SAT at the price of increasing complexity (as L_r approaches L). Further, SAT exhibits self-calibrating capability and robustness to transmit-receive filter mismatch caused by phase errors, pulse distortions, mis-calibrated antennas and unmodelled channel dynamics, simply because it utilizes the aggregate template $p_R(t)$ instead of $p_T(t)$ that the RAKE relies on. Recall that with $L_r < L$, the RAKE does not possess asymptotic optimality. Both robustness and the low-complexity features of SAT are particularly attractive for UWB receivers, where L can be in the order of hundreds and the ultra-short monocycle is vulnerable to transmitter-receiver mismatch [17]. Notice that by incorporating phase errors in p_R, SAT-based demodulation obviates the need for phase synchronization.

To appreciate the merits of our blind synchronization and demodulation schemes in multi-user ad hoc access, let us outline the *overall protocol* we envision for a wireless sensor network (WSN) setting. With reference to Figure 1, the master node A broadcasts regularly to its cluster zero-mean BPSK information symbols and occasionally information symbols obeying the synchronization pattern in C3. An idle neighbor node B "wakes up" and starts averaging the $r(t)$ it receives from node A according to (5). Its $\bar{r}(t)$ becomes effectively nonzero when the synchronization pattern is broadcasted, at which time node B uses (9) and (11) to synchronize and demodulate blindly even in the presence of MUI coming from nodes belonging to the same or other clusters. Meanwhile, nodes with established links in the same cluster with A (e.g., node C) receive information without interruption which they demodulate using the detector in (11). During the synchronization phase, node C does not change its demodulation scheme but its BER improves slightly when demodulating nonzero mean information symbols since $\theta > 1$. On the other hand, nodes belonging to other clusters (pico-nets) view node A as MUI and their BER degrades slightly when node A broadcasts nonzero-mean symbols.

IV. Performance Analysis

The objective here is to analyze the impact $\hat{\tau}_0$ and $\hat{p}_R(t)$ in (9) have on the BER performance of the demodulator in (11). Starting with $\bar{r}(t)$ in (5), it is easy to check that the conditions for applying the law of large numbers in [3] are satisfied here, ensuring that $\bar{r}(t)$ is mss consistent; i.e., $\lim_{N\to\infty} \bar{r}(t) \overset{mss}{=} \mathsf{E} r(t)$ for $t \in [0, MT_s]$. Since well behaved functions of consistent estimators are themselves consistent, the latter implies that $\lim_{N\to\infty} \hat{\tau}_0 \overset{mss}{=} \arg\max_{\tau\in[0,MT_s)} J(\tau) := \tau_0$ and $\lim_{N\to\infty} \hat{p}_R(t) \overset{mss}{=} p_R(t)$, meaning that $\hat{\tau}_0$ and $\hat{p}_R(t)$ are indeed mss consistent. The implication is that for N sufficiently large, our SAT-based matched filter demodulator effectively operates with $p_R(t)$ and thus collects the full energy of the channel. This endows our SAT receiver with: i) asymptotic ML optimality when both MUI and ISI are absent; ii) asymptotic optimality in the maximum SNR sense when MUI is absent but ISI is present; and iii) asymptotic optimality in the maximum signal-to-interference-plus-noise ratio (SINR) sense, when both MUI and ISI are present. Recall that with $L_r < L$, the RAKE does not possess optimality even when the number of training symbols approaches infinity. In summary, we have shown that:

Proposition 3: *The timing and SAT estimators in (9) are mss consistent. Asymptotically (as $N \to \infty$), the demodulator in (11) collects the maximum possible energy and thus upper bounds the BER performance of the RAKE receiver.*

To further delve into the BER performance, let us start by defining $\bar{\eta}(t)$, $\bar{\rho}(t)$ and $\{\bar{S}_m\}_{m=0}^{M-1}$ sample averages as $\bar{r}(t)$ in (5), after replacing $r(t)$ with $\eta(t)$, $\rho(t)$ and $s(nM+m)$, respectively; e.g., $\bar{S}_0 := N^{-1}\sum_{n=0}^{N-1} s(nM)$. Substituting (3) into (5) and using these definitions, for $t \in [0, MT_s]$, we show in Appendix B that $\bar{r}(t)$ can be expressed for N sufficiently large as:

$$\begin{aligned}\bar{r}(t) &= \sqrt{\mathcal{E}}\bar{S}_0 \sum_{l=0}^{1} p_R(t + lMT_s - \tau_0) + \bar{\eta}(t) + \bar{\rho}(t) \\ &+ \sqrt{\mathcal{E}} \sum_{m=1}^{M-1} \bar{S}_m \sum_{k=0}^{2} p_R(t + (kM - m)T_s - \tau_0). \quad (12)\end{aligned}$$

There are two sources of error in Eq. (12): one captures combined MUI plus AWGN effects; while the other emerges due to finite averaging (N segments). We will henceforth

view MUI as part of the AWGN, and pursue asymptotic BER analysis in two directions: i) when N is large; and ii) when the SINR is large.[4] Since MUI is neither white nor Gaussian, the BER expressions in the remainder of this section should be viewed as optimistic bounds of the expected performance in practice. This approximation will be quantified with realistic simulations in Section VI.

A. Large Sample Performance

Let us consider (9) for N large. Although the offsets τ searched can be anywhere in $[0, MT_s)$, the mss consistency of $\hat{\tau}_0$ guarantees that for N sufficiently large, we will have $|\tau_0 - \hat{\tau}_0| \leq T_s$; i.e., we will be sufficiently close to the true τ_0. Similarly, the estimated SAT will satisfy $\hat{p}_R(t) = (\sqrt{\mathcal{E}}\mu_0)^{-1}\mathsf{E}r(t+\hat{\tau}_0) = \sum_{k=-1,0 \text{ or } k=0,1} p_R(t+kMT_s-\tau_0+\hat{\tau}_0)$ with $t \in [0, T_R]$. But for $|\tau_0-\hat{\tau}_0| \leq T_s$, only the summand corresponding to $k=0$ contributes, and we arrive at:

$$\hat{p}_R(t) = p_R(t - \tau_0 + \hat{\tau}_0),\ t \in [0, T_R]. \tag{13}$$

Using (13) in the correlation involved in (10), we obtain $\phi_{\hat{p}_R p_R}(n;\tilde{\tau}_0) = \int_0^{T_R} p_R(t-\tilde{\tau}_0)p_R(t-nT_s-\tilde{\tau}_0)dt$. Notice that when $n \notin [-(M-2), M-2]$, we have $\phi_{\hat{p}_R p_R}(n;\tilde{\tau}_0) = 0$; while setting $n=0$, yields the energy captured by the estimated SAT that we define as: $E_C(\tilde{\tau}_0) := \int_0^{T_R} p_R^2(t-\tilde{\tau}_0)dt$. Now recall that the noise subsumes MUI, and abbreviate the sum in (10) as $ISI(k) := \sqrt{\mathcal{E}}\sum_{n=-(M-2),n\neq 0}^{M-2} \phi_{\hat{p}_R p_R}(n;\tilde{\tau}_0)s(k+n)$. Taking all these into account, the detection statistic implied by the mss consistency of $\hat{\tau}_0$ and $\hat{p}_R(t)$ for N sufficiently large, is given by:

$$d(k) = \sqrt{\mathcal{E}}E_C(\tilde{\tau}_0)s(k) + ISI(k) + \eta(k;\tilde{\tau}_0)\ , \tag{14}$$

where $\eta(k;\tilde{\tau}_0) := \int_0^{T_R} p_R(t-\tilde{\tau}_0)\eta(t+kT_s+\hat{\tau}_0)dt$ is zero mean AWGN with variance $E_C(\tilde{\tau}_0)N_0/2$ (see Appendix C). Notice that $ISI(k)$ is a finite-valued random variable since it involves $2(M-2)$ random symbols; e.g., if $s(n)$ is BPSK, then $ISI(k)$ can take any of $2^{2(M-2)}$ equiprobable values, each corresponding to a different combination of the (here binary) symbols $\{s(k+n),\ n \in [-M+2, M-2],\ n \neq 0\}$.

The BER when demodulating $s(k)$ from the $d(k)$ in (14) can be evaluated in two steps: i) find the BER conditioned on each realization of $\{s(k+n)\}_{n=-(M-2),\neq 0}^{M-1}$; and ii) average over all possible $\{s(k+n)\}_{n=-(M-2),\neq 0}^{M-1}$ combinations. During the first step, $ISI(k)$ is a constant and evaluating performance of the detection problem in (14) is straightforward. When $s(k)$ is binary, the solution is given by the well known simple closed-form in terms of the Gaussian tail (Q) function:

$$P_e = \frac{1}{2^{2(M-2)}} \sum_{ISI(k)\in\mathcal{A}_{ISI}} Q\left(\sqrt{\frac{2\mathcal{E}E_C(\tilde{\tau}_0)}{N_0}} + \frac{\sqrt{2}ISI(k)}{\sqrt{E_C(\tilde{\tau}_0)N_0}}\right)\ , \tag{15}$$

where $\mathcal{A}_{ISI}$ denotes the finite alphabet of the $ISI(k)$ term, and the averaging corresponds to the aforementioned step ii). As an immediate corollary of (15), we can set $M=2$ and find the BER for the ISI-free case with BPSK:

$$P_e = Q\left(\sqrt{\frac{2\mathcal{E}E_C(\tilde{\tau}_0)}{N_0}}\right)\ . \tag{16}$$

Although explicit forms are shown here only for BPSK, the general result is as follows:

Proposition 4: *For N large enough to ensure $|\tau_0 - \hat{\tau}_0| \leq T_s$, the BER incurred by the SAT-based slicer (11) in the presence of zero-mean AWGN is computable and depends on the severity of ISI and the energy captured by the estimated SAT. For binary constellations, the BER is given by (15) [(16)] in the presence [absence] of ISI.*

A point worth emphasizing is the BER dependence on the energy capture $E_C(\tilde{\tau}_0)$ that matters more than the accuracy of $\hat{\tau}_0$. Indeed, even when the error $\tilde{\tau}_0$ is relatively high, if E_C captures most of the E_R energy, the resultant BER will be low; see also [20]. This is important since after all the goal is reliable demodulation rather than "super-accurate" synchronization.

B. High SINR Performance

To isolate and study separately the effect of finite averaging on BER, we consider here the high SINR (practically free of MUI, ISI and AWGN) performance of our sign detector which depends on $\hat{\tau}_0$ and $\hat{p}_R(t)$. Our starting point is again (12), where we set $\bar{\eta}(t) = \bar{\rho}(t) = 0$; and since in the ISI-free case C2 suggests $M=2$, we can simplify $\bar{r}(t)$ for $t \in [0, 2T_s]$ as:

$$\begin{aligned}\bar{r}(t) &= \sqrt{\mathcal{E}}\bar{S}_0 \sum_{k=0}^{1} p_R(t+2kT_s-\tau_0) \\ &+ \sqrt{\mathcal{E}}\bar{S}_1 \sum_{k=0}^{2} p_R(t+(2k-1)T_s-\tau_0)\ .\end{aligned} \tag{17}$$

The timing estimator in (9) uses $\bar{r}(t)$ to obtain: $\hat{\tau}_0 = \arg\max_{\tau\in[0,2T_s)} \bar{J}(\tau)$, where $\bar{J}(\tau) := \int_0^{T_R} \bar{r}^2((t+\tau)_{\text{mod } 2T_s})dt$. Notice that the shifted replicas of the SAT involved in $\bar{r}^2(t+\tau)$ are $\{p_R(t+iT_s+\tau-\tau_0)\}_{i=-1}^{3}$. Since both τ and τ_0 belong to $[0, 2T_s)$, it follows that $\tau-\tau_0 \in (-2T_s, 2T_s)$; which implies that the SAT replica corresponding to $i=3$ is shifted by $3T_s+\tau-\tau_0 \in (T_s, 5T_s)$, and thus falls out of the integration range in $\bar{J}(\tau)$ since $T_R \leq T_s$ here. Furthermore, even the remaining SAT copies (that have duration $T_R \leq T_s$), are at least T_s-apart; hence, they do not overlap, and the square of their weighted sum in $\bar{r}^2$ equals the sum of their weighted squares. These considerations, allow us to simplify $\bar{J}(\tau)$ to:

$$\begin{aligned}\bar{J}(\tau) &= \mathcal{E}\int_0^{T_R} \Big[\bar{S}_0^2 \sum_{k=0}^{1} p_R^2(t+2kT_s+\tau-\tau_0)dt \\ &+ \bar{S}_1^2 \sum_{l=\pm 1} p_R^2(t+lT_s+\tau-\tau_0)\Big]dt\ .\end{aligned} \tag{18}$$

We wish to show that $\bar{J}(\tau)$ exhibits a unique maximum at $\tau=\tau_0$ for any finite N. To this end, we suppose $\bar{S}_0^2 > \bar{S}_1^2$, which even for moderate N will hold with high probability since $\bar{S}_0$ will approximate the nonzero mean μ_0, whereas $\bar{S}_1$ will be close to zero, as it corresponds to the average of zero mean symbols. Under this realistic assumption, recall that $\tau-$

[4] With the non-Gaussian distribution and color of MUI unknown, analytical BER expressions are otherwise impossible.

$\tau_0 \in (-2T_s, 2T_s)$, and consider first that $\tau - \tau_0 \in (0, T_s)$. Careful consideration of the integration range in (18) shows that:

$$\begin{aligned}\bar{J}(\tau) &\leq \mathcal{E}\left[\bar{S}_0^2 \int_{\tau-\tau_0}^{T_R} p_R^2(t)dt + \bar{S}_1^2 \int_0^{\tau-\tau_0} p_R^2(t)dt\right] \\ &< \mathcal{E}\bar{S}_0^2 \int_0^{T_R} p_R^2(t)dt := \bar{J}(\tau_0) \ .\end{aligned}$$

This proves that $\bar{J}(\tau)$ is maximized at $\tau = \tau_0$ when $\tau - \tau_0 \in [0, T_s)$; and arguing similarly, the same can be shown for the other intervals in $(-2T_s, 2T_s)$ that $\tau - \tau_0$ belongs to.

With the synchronizer yielding deterministically (for $\bar{S}_0^2 > \bar{S}_1^2$) the correct timing offset, the SAT estimator in (9) for this high-SINR regime will be: $\hat{p}_R(t) = (\bar{S}_0/\mu_0)p_R(t)$; and the decision statistic in (10) will simplify to: $d(k) = (\sqrt{\mathcal{E}}E_R\bar{S}_0/\mu_0)s(k)$. With noise and interference absent, the only source of uncertainty in this simple form of $d(k)$ is $\bar{S}_0$. For the sign detector (11) in particular, we will have an error if a negative $\bar{S}_0$ alters the sign of $d(k)$; i.e., $P_e = \mathsf{Pr}(\bar{S}_0 < 0)$. This makes BER evaluation of the demodulator easy because the central limit theorem allows us to consider $\bar{S}_0$ as approximately Gaussian with known mean and variance, even for small sample sizes (say $N \leq 20$). For our asymmetric BPSK paradigm, we have $\mathsf{E}(\bar{S}_0) = (\theta - 1)/2$ and $\mathsf{Var}(\bar{S}_0) = N^{-1}[(\theta + 1)/2]^2$. Using these parameters, the BER can be computed in closed form in terms of the Q-function as:

$$P_e \cong Q\left(\sqrt{N}\ \frac{\theta - 1}{\theta + 1}\right) \ . \tag{19}$$

We are now ready to summarize our result for the high SINR case:

Proposition 5: *As SINR goes to ∞, $\hat{\tau}_0$ in (9) approaches τ_0. The two coincide deterministically even for N finite and small, so long as $\bar{S}_0^2 > \bar{S}_1^2$. The approximate BER of the resultant sign detector can be computed, and for the binary case it assumes the closed form in (19).*

The fact that BER in (19) does not depend on $\sqrt{\mathcal{E}}E_R$ is not as surprising since we assumed infinite SINR. On the other hand, we see that BER at high SINR can be lowered either through increasing the nonzero mean (making the asymmetry stronger by choosing $\theta \gg 1$), or, by longer averaging (larger N), even when the asymmetry is minimal (small $(\theta-1)/(\theta+1)$ ratio).

V. Decision-Directed Algorithms

The timing and SAT estimators in (9) were obtained by exploiting the cyclostationarity enabled by the nonzero mean symbols during the synchronization phase. The latter lasts for only a small fraction (say $< 5\%$) of the time during which only zero-mean symbols are "in the air." Because this span of zero-mean information symbols may well exceed the channel's coherence time, the need arises to track $\hat{\tau}_0$ and $\hat{p}_R(t)$, and develop adaptive demodulators capable of accounting for channel variations. This motivates the first goal of this section to derive decision-directed (DD) tracking algorithms for updating $\hat{\tau}_0$, $\hat{p}_R(t)$ and $\hat{s}(k)$ every K symbols. How small the block size K is chosen relative to $K_{coh} := \lceil T_{coh}/T_s \rceil$ depends on tradeoffs among tracking, accuracy and complexity.[5] Our second goal here is to develop low-complexity DD alternatives with improved performance during the synchronization phase.

Let us consider the cross-correlation $\phi_{sr}(t) := \mathsf{E}[s(n)r(t + nT_s)]$, and substitute $r(t + nT_s)$ from (3). Since symbols $\{s(n)\}$ are zero mean and uncorrelated, it follows easily that

$$\phi_{sr}(t) = \sqrt{\mathcal{E}}\ \mathsf{E}[s^2(n)]\ p_R(t - \tau_0) \ , \tag{20}$$

where the mean-square $\mathsf{E}[s^2(n)]$ coincides here with the symbol variance σ_s^2 (= 1 for PSK constellations). The equality (within a scale) of $\phi_{sr}(t)$ in (20) with a period of $\mathsf{E}r(t)$ in (4) proves readily our first *key result* to be used outside the synchronization phase [c.f. (9)]:

$$\begin{aligned}\tau_0 &= \arg \max_{\tau \in [0, T_s)} \int_0^{T_R} \phi_{sr}^2(t + \tau)dt \ , \\ p_R(t) &= \frac{1}{\sqrt{\mathcal{E}}\sigma_s^2}\ \phi_{sr}(t + \tau_0),\ t \in [0, T_R] \ ;\end{aligned} \tag{21}$$

namely, that timing and SAT recovery in the presence of ISI and MUI is possible based on $\phi_{sr}(t)$. Notice that since $\phi_{sr}(t)$ relies on $r(t)$ that is cyclostationary with period T_s (rather than $\bar{r}(t)$ that has period MT_s), the search for the maximum τ_0 in (21) is confined w.l.o.g. in $[0, T_s)$.

As with (5), if K symbols $s(n)$ were available, mss consistent estimation of $\phi_{sr}(t)$ would have been possible using $K^{-1}\sum_{n=0}^{K-1} s(n)r(t + nT_s)$, $t \in [0, MT_s]$. As usual, the crux of DD tracking and adaptive demodulation algorithms is to have already detected symbols $\hat{s}(n)$ replace $s(n)$ in this sample average. With b indexing blocks of size K, let us write $n = bK + k$ with $k \in [0, K - 1]$, and suppose that $\hat{\tau}_0^{(b-1)}$ and $\hat{p}_R^{(b-1)}(t)$ are available. Relying on these timing and SAT estimates, we can detect the bth block's BPSK symbols using [c.f. (11)]: $k \in [0, K - 1]$,

$$\hat{s}(bK + k) = \mathsf{sign}\Big[\int_0^{T_R} \hat{p}_R^{(b-1)}(t)r(t + \hat{\tau}_0^{(b-1)} + (bK + k)T_s)dt\Big] \ . \tag{22}$$

Based on $\{\hat{s}(bK + k)\}_{k=0}^{K-1}$ decisions, we can then estimate the cross-correlation via

$$\hat{\phi}_{sr}^{(b)}(t) = \frac{1}{K}\sum_{k=0}^{K-1} \hat{s}(bK + k)r(t + (bK + k)T_s),\ t \in [0, MT_s] \ . \tag{23}$$

If SAT information becomes outdated and an update is desired in the ensuing block b, we simply replace the needed ensemble cross-correlation in (21) by its sample estimate from (23) to obtain:

$$\begin{aligned}\hat{\tau}_0^{(b)} &= \arg \max_{\tau \in [0, T_s)} \int_0^{T_R} [\hat{\phi}_{sr}^{(b)}(t + \tau)]^2 dt \ , \\ \hat{p}_R^{(b)}(t) &= \frac{1}{\sqrt{\mathcal{E}}\sigma_s^2}\ \hat{\phi}_{sr}^{(b)}(t + \hat{\tau}_0^{(b)}) \ ;\end{aligned} \tag{24}$$

For the next iteration, simply increment b to $b + 1$ and use (22) only to continue demodulation, or, (22)-(24) whenever a SAT update is also needed.

[5] As with the delay-spread, T_{coh} is readily computable from an upper bound on the channel's Doppler-spread that is assumed available through channel sounding experiments.

If a sufficiently large number of $\hat{s}(bK+k)$ decisions are correct in (23), then $\hat{\phi}_{sr}^{(b)}(t)$ will converge in the mss to the true $\phi_{sr}(t)$ as K increases. Arguing as in Section IV, this implies that the DD timing and SAT estimators in (24) are mss consistent as $K \to \infty$, which in turn establishes that the MUI- and ISI-resilient DD demodulator in (22) enjoys the asymptotic optimality properties we summarized in Proposition 3 for the blind detector in (11).

Apart from tracking *outside* the synchronization phase, DD alternatives can be very attractive to considerably enhance the performance of SAT recovery *during* synchronization, as we alluded to in Remark 1. To prove this, recall the synchronization pattern in C3 and consider the cross-correlation now defined as $\phi_{sr}(t) := \mathsf{E}[s(kM)r(t+kMT_s)]$. Because the symbols $s(kM)$ have nonzero mean, substituting $r(t+kMT_s)$ from (3) yields:

$$\phi_{sr}(t) = \sqrt{\mathcal{E}}\,\mathsf{E}[s^2(kM)]\,p_R(t-\tau_0)\ , \tag{25}$$

where we used that in addition to being mutually uncorrelated, $\{s(kM)\}$ are uncorrelated with the zero mean symbols $\{s(kM+m)\}_{m=1}^{M-1}$ (which annihilates the ISI), with the zero-mean $\rho(t)$ (which suppresses MUI) and with the zero mean $\eta(t)$ (which mitigates AWGN). If the nonzero mean $s(kM)$ are asymmetric BPSK symbols, then $\mathsf{E}[s(kM)] = (\theta-1)/2$ and $\mathsf{E}[s^2(kM)] = (\theta^2+1)/2$.

Compared with (20) and (4), $\phi_{sr}(t)$ in (25) shows an analogous form, except for a seemingly minor difference in the scaling factor. But this analogy has three major implications:

i) Timing and SAT estimation, SAT-based demodulation and their optimality summarized in Propositions 1-3 for the $\bar{r}(t)$ based algorithms, apply to analogous schemes that become available via the mss consistent estimator: $\hat{\phi}_{sr}(t) = N^{-1}\sum_{n=0}^{N-1} s(nM)r(t+nMT_s)$;

ii) Relative to $\bar{r}(t)$ based estimators in Section III, the performance of those based on $\hat{\phi}_{sr}(t)$ is enhanced due to considerable SNR gains. In the binary case, this comes from the gain difference ($(\theta^2+1)/2$ versus $(\theta-1)/2$), which increases SNR by a factor of $2(\theta^2+1)/(\theta-1)^2$;

iii) The corresponding algorithms based on $\hat{\phi}_{sr}(t)$ apply during the synchronization phase, not only when $\{s(nM)\}_{n=0}^{N-1}$ are known through training, but also iteratively in a DD mode using (22)-(24), where now the superscript (b) stands for iteration number.

Interestingly, these attractive features can be effectively retained in the DD synchronization phase even with a variant of the cross-correlation approach that has complexity as low as the $\bar{r}(t)$ approach. Let the subscript $\pm$ denote sign-only quantities, and consider the cross-correlation $\phi_{rs_\pm}(t) := \mathsf{E}[s_\pm(kM)r(t+kMT_s)]$, where for binary symbols $s_\pm(kM) := \mathsf{sign}[s(kM)]$. Arguing as in (20) and (25), it follows that: $\phi_{rs_\pm}(t) = \sqrt{\mathcal{E}}\mathsf{E}[s_\pm(kM)s(kM)]\,p_R(t-\tau_0)$, where for asymmetric BPSK symbols $\mathsf{E}[s_\pm(kM)s(kM)] = (\theta+1)/2$. The latter will increase SNR by a factor of $(\theta+1)^2/(\theta-1)^2$, when estimation of τ_0 and $p_R(t)$ is aided by $s_\pm(kM)$.

Initialized with the $\bar{r}(t)$ based estimates $\hat{\tau}_0$, $\hat{p}_R(t)$, the recommended DD algorithm for the synchronization phase first detects the nonzero mean symbols' sign [c.f. (11) and (22)]:

$$\hat{s}_\pm(kM) = \mathsf{sign}\left[\int_0^{T_R} \hat{p}_R(t)r(t+\hat{\tau}_0+kMT_s)dt\right]\ . \tag{26}$$

These $\{\hat{s}_\pm(nM)\}_{n=0}^{N-1}$ signs allow forming the sample correlation estimate:

$$\hat{\phi}_{rs_\pm}(t) = \frac{1}{N}\sum_{n=0}^{N-1}\hat{s}_\pm(nM)r(t+nMT_s)\ . \tag{27}$$

Because the multiplication per summand is just with a sign, the complexity in implementing $\hat{\phi}_{rs_\pm}(t)$ is comparable to that of $\bar{r}(t)$ in (5), which is already very low.

Similar to (24), the DD SAT estimates are:

$$\begin{aligned}\hat{\tau}_0^{dd} &= \arg\max_{\tau\in[0,T_s)}\int_0^{T_R}[\hat{\phi}_{rs_\pm}(t+\tau)]^2dt\ ,\\ \hat{p}_R^{dd}(t) &= \frac{1}{\sqrt{\mathcal{E}}\sigma_s^2}\,\hat{\phi}_{rs_\pm}(t+\hat{\tau}_0)\ .\end{aligned} \tag{28}$$

Although iterations are possible, one DD pass suffices in practice and keeps the complexity low. We close by summarizing the results of this section:

Proposition 6: *Under C1-C4, block-adaptive DD timing estimation, SAT recovery and demodulation can be implemented outside the synchronization phase using (22)-(24) to track channel variations. During the synchronization phase, DD timing estimation, SAT recovery and demodulation enhance performance at low complexity especially when implemented using sign-only decision information as in (26)-(28). All DD algorithms enjoy the asymptotic optimality properties summarized in Proposition 3 for their non-DD counterparts.*

VI. Simulations

In this section, we simulate the synchronization and demodulation schemes of Section III and their DD enhancements of Section V. Our simulations focus on UWB systems. Throughout, BPSK symbols modulate the so called Gaussian (monocycle) pulse shaper $p(t) = 2\sqrt{e}A(t/\tau_g)\exp(-2t^2/\tau_g^2)$ with $\tau_g = 0.2$ ns; in asymmetric BPSK, we use $\theta = 3$. The multipath channel is "CM 1" from the IEEE 802.15.3a working group [6], having mean excess delay 4.9 ns and RMS delay spread 5 ns. We have verified experimentally that the delay spread of CM1 is effectively upper bounded by 29 ns. After truncation to 29 ns, the channel is normalized to have unit power gain. Simulated performance curves are obtained by averaging 100 random system realizations. For each realization, we first acquire the timing and recover the SAT as in (9). Based on the SAT, we subsequently demodulate as in (10) and (11). Per realization, BER for the sign detector in (11) is analytically calculated by enumerating all possible values of the interference terms.

A. SAT Acquisition and Demodulation Performance

Test A. ISI Absent: To avoid ISI, we select $T_f = 30$ns, $N_f = 10$, $T_c = 3$ns and $c_9 = 0$; the spreading codes $\{c_k\}_{k=0}^{8}$ are randomly generated taking values from $\{0,1,\ldots,9\}$. We implemented (9) and (11) with $M = 2$. Figs. 3 and 4 illustrate timing acquisition and BER performance across SNR in the

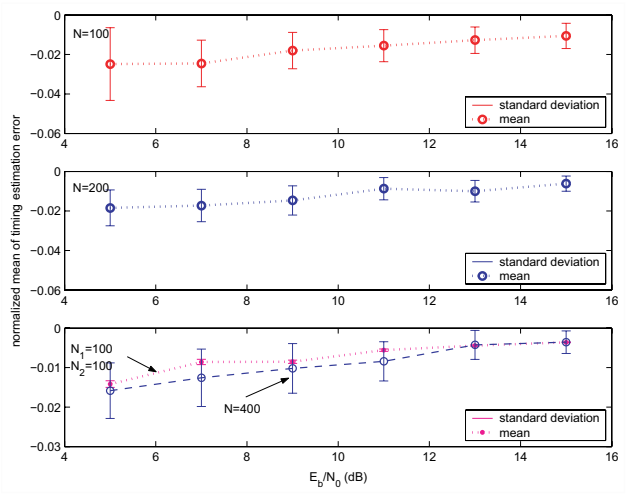

Fig. 3. Normalized (with respect to T_s) mean $\pm$ half of the standard deviation of the timing estimation errors when ISI and MUI are absent.

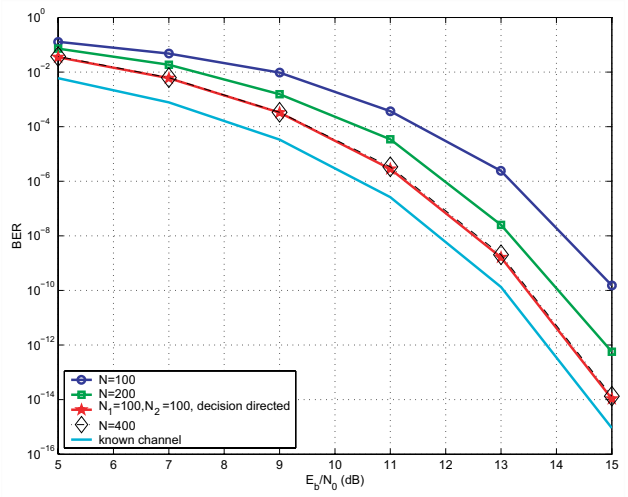

Fig. 4. BER performance when ISI and MUI are absent.

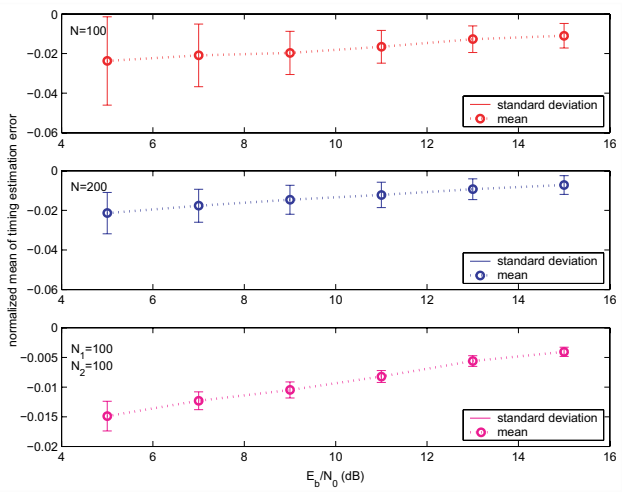

Fig. 5. Normalized (with respect to T_s) mean $\pm$ half of the standard deviation of the timing estimation errors when ISI is absent but MUI is present (MUI is caused by two asynchronous nodes with the same power).

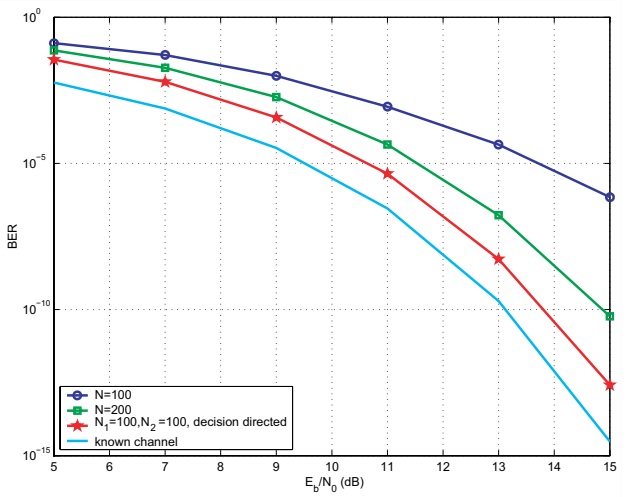

Fig. 6. BER performance when ISI is absent but MUI is present (MUI is caused by two asynchronous nodes with the same power).

absence of MUI; their counterparts when MUI is present are shown in Figs. 5 and 6.

Test B. ISI Present: Spreading codes are generated as before, but here we select $T_f = 10$ns, $N_f = 10$ and $T_c = 1$ns to induce ISI. Using $M = 3$ in C2, the results of implementing (9) and (11) are depicted in Figs. 7 and 8 when MUI is absent; and correspondingly in Figs. 9 and 10, when MUI is present.

For the DD algorithms, we acquired initial timing and SAT estimates using (5) and (9), with $N = N_1 = 100$. Subsequently, we employed (26), (27) and (28) with $N = N_2 = 100$ additional periods to improve the timing and SAT estimates in a DD mode. The DD curves are shown in the aforementioned figures along with their non-DD counterparts. Observe that in Fig. 4, the non-DD curve corresponding to $N = 400$ nearly coincides with the DD one corresponding to $N_2 = 100$. This corroborates our claim that the DD approach increases the SNR (with $\theta = 3$, the DD algorithm in (27) increases the SNR by a factor of $[(\theta+1)/(\theta-1)]^2 = 4$).

From these simulations, one can verify that with reasonable averaging (N), our SAT receiver will be only $1-2$dBs away from the clairvoyant one (with perfectly known timing and channel).

B. Performance of Decision-Directed Tracking

Here we use $T_f = 30$ns, $N_f = 10$, $T_c = 3$ns, $c_9 = 0$ and generate the random time hopping codes as before. We will not consider MUI, even though we have successfully tested our algorithms with MUI too. As discussed in [7], the anticipated speed of moving users in a typical UWB scenario is about $v = 1$ m/s, which implies that the rate of channel variation is upper bounded by 3 ns per second. With maximum carrier frequency $f_c = 6$ GHz, the maximum Doppler spread is: $f_D = v/(c/f_c) = (6 \times 10^9)/(3.0 \times 10^8) = 20$ Hz. The channel coherence time is then about [16, Chap. 4]: $T_{coh} = 0.423/f_D = 21$ ms, which corresponds to about $\lceil T_{coh}/T_s \rceil = 70,000$ symbols. Fig. 11 depicts the performance of our DD tracker based on (22)-(24) with $K = 100, 200, 400$ and bit-energy-to-noise ratio 20 dB. Notice that it suffices to perform timing and SAT updates, based on (23) and (24), only once every $K_{coh} = \lceil T_{coh}/T_s \rceil = 70,000$ symbols.

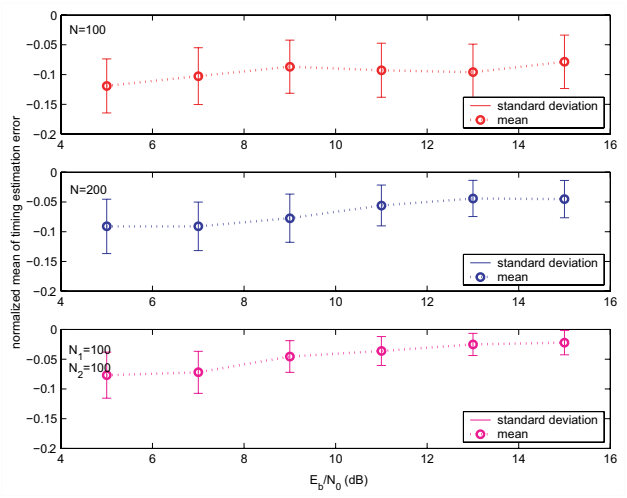

Fig. 7. Normalized (with respect to T_s) mean $\pm$ half of the standard deviation of the timing estimation errors when MUI is absent but ISI is present.

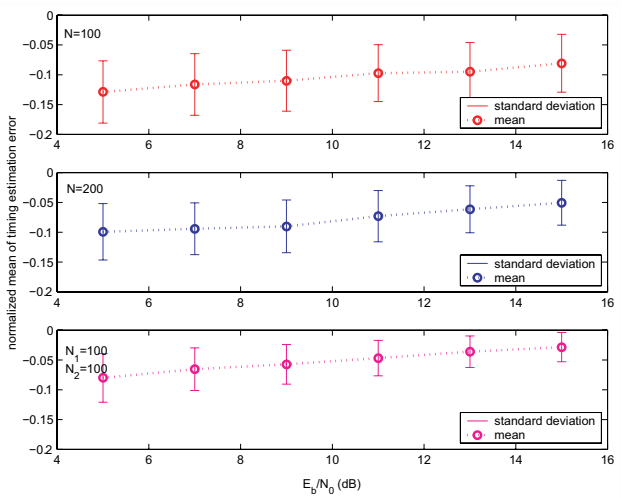

Fig. 9. Normalized (with respect to T_s) mean $\pm$ half of the standard deviation of the timing estimation errors when both MUI and ISI are present.

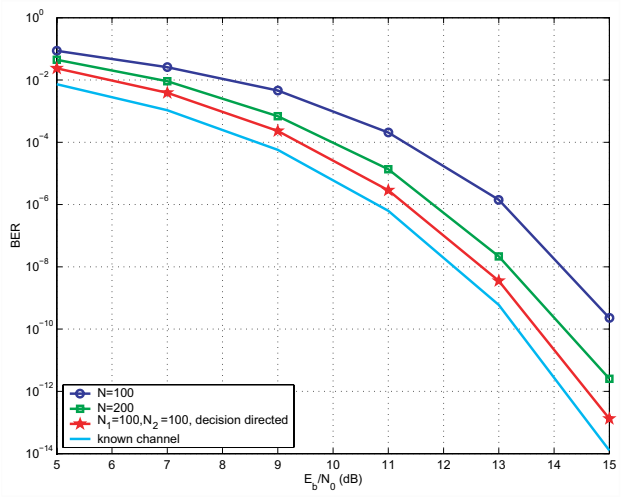

Fig. 8. BER performance when MUI is absent but ISI is present.

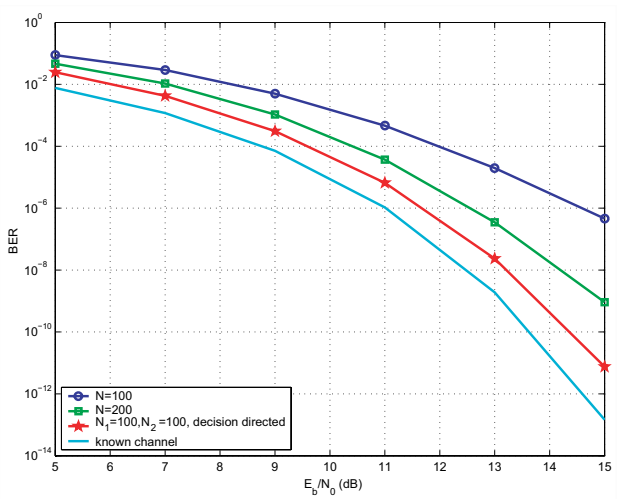

Fig. 10. BER performance when both MUI and ISI are present.

VII. Concluding Summary and Discussion

We derived a transmission protocol along with receiver algorithms for low-complexity blind timing acquisition, tracking and demodulation based on a synchronized aggregate template (SAT). The latter captures transmit-filter, phase errors, pulse distortion, ISI and unmodelled receiver effects, all of which are allowed to be unknown. The key idea was to transmit periodically, during the synchronization phase, nonzero mean symbols with period exceeding (by a symbol period) a known upper bound of the SAT's nonzero support. Periodically inserted nonzero mean symbols induced first order cyclostationarity, which in turn enabled blind estimation of the aggregate template (within a circular shift) using the sample mean of the received waveform. The symbol-long guard time allowed us to resolve the circular shift (i.e., estimate the timing offset) via low-complexity energy detection, and thus recover the SAT blindly.

Our novel demodulator matched to the SAT has great potential for deployment in future generation systems. Whether implemented digitally or as an analog filter, the SAT-based demodulator alters the line of constructing receivers in the presence of ISI by aiming at SAT recovery which suffices for reliable demodulation without being necessary to perform costly channel estimation. Indeed, our blind SAT offers not only robustness relative to the popular RAKE receiver, but also exhibits improved performance at lower complexity because it avoids the approximation emerging with a reduced number of RAKE fingers while at the same time it completely avoids estimation of the channel taps and delays needed when designing a RAKE receiver. Performance analysis quantified how the nonzero mean of synchronization symbols and the averaging time used to form the SAT affect bit error rate performance. It also revealed that for sufficiently long averaging times, what matters is the energy captured in the SAT and not necessarily the accuracy of the timing estimate itself. Further analytical and simulation based comparisons between SAT and RAKE can be found in [10], where our timing estimator and SAT-based demodulator are generalized to accommodate pulse-position modulation (PPM) too.

Having a single (but not necessarily the same) node transmitting the synchronization pattern of nonzero mean (but otherwise unknown) symbols, enabled simultaneous communica-

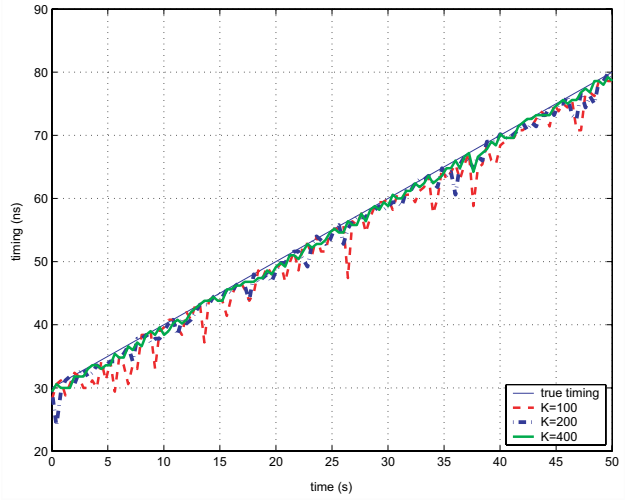

Fig. 11. Tracking capability of the block-adaptive DD timing estimator.

tion (with zero mean symbols) among already synchronized nodes. This endows our scheme with two more benefits: MUI resilience both in fixed (e.g., cellular) architectures as well as in ad hoc networks with cluster-heads or gateways acting as synchronizers. In cellular CDMA systems for example, the base station can synchronize one user at a time without pausing reception of other users in normal communication mode, regardless of the ISI present – a challenging problem welcoming such a low-complexity blind solution. Likewise, our blind synchronization and low-complexity demodulation is welcomed in ad hoc access systems and wireless sensor networks in particular, where resources and cost are at a premium. Our approach here requires only a single node transmitting the nonzero mean synchronization pattern. If two or more nonzero mean signals are "in the air," MUI can be suppressed by separating nodes in the frequency-domain. This can be accomplished using for instance the multi-band pulse shaper designs in [11].

As a closing note, we should re-iterate that our acquisition, tracking and demodulation schemes find universal applicability to a broad spectrum of narrowband, wideband or UWB modalities transmitted over AWGN or ISI-inducing wireless channels, and processed by low-complexity coherent receivers. UWB multi-user ad hoc access is a paradigm where all benefits appear jointly: low complexity blind operation with resilience to MUI and ISI. These features were verified in our simulations which also illustrated that with practical averaging times used to recover the SAT, bit error rates in UWB systems are only $2dB$ off the ideal curves corresponding to perfectly known timing offsets and channels. The price paid for these nice features is increase in power needed to effect the nonzero mean property. In tactical communications this may raise the probability of detection by the adversary. But fortunately, it can be kept to minimal levels by increasing the averaging in estimating the SAT. More important, this increase is small since it is present in a few symbols and only during the synchronization phase. Finally, the nonzero mean offers the simplest means of inducing cyclostationarity, which is a must for timing synchronization.

Appendix A: Upper Bound on the Channel Delay-Spread

In our operating condition C2 we assumed that the SAT duration T_R is known, which is possible when the channel delay spread $\tau_{L,0}$ is exactly known. However, M can still be selected as in C2 even when only an upper bound on T_R is available. In this case, we select M to satisfy $T_R \leq (M-1)T_s$, and replace all integration limits involving T_R with $(M-1)T_s$ which now bounds T_R. With this change, the objective in (8) becomes $J'(\tau) = \int_0^{(M-1)T_s} \sum_n p_R^2(t - nMT_s + \tau - \tau_0)dt$. But different from (8), where τ_0 is the *unique* maximum point, the gap $(M-1)T_s - T_R > 0$ renders $J'(\tau)$ possess *a unique set* of maxima. Because of this, the timing offset becomes identifiable by peak-picking $J'(\tau)$ only within a set. Specifically, it is tedious but straightforward to show that: i) if $\tau_0 \geq (M-1)T_s - T_R$, then $\arg\max_{\tau\in[0,MT_s)} J'(\tau) \in [\tau_0 - ((M-1)T_s - T_R), \tau_0]$; and if $\tau_0 < (M-1)T_s - T_R$, then $\arg\max_{\tau\in[0,MT_s)} J'(\tau) \in [0,\tau_0] \cup [\tau_0 - ((M-1)T_s - T_R) + MT_s, MT_s)$.

Fortunately, this set uniqueness does not affect the performance of $\hat{\tau}_0$ and $\hat{p}_R(t)$ that are still obtained (integration over $[0,(M-1)T_s]$) as in (9). The reason is that for any estimated timing offset in the set, $\bar{r}((t+\hat{\tau}_0)_{\text{mod } MT_s})$ still captures essentially the same (asymptotically the maximum) energy available. Thus, all asymptotic optimality properties we proved for the timing and SAT estimators as well as for the resultant demodulator, carry over when only an upper bound on T_R is available. Of course, mss consistency now refers to a convergence in a set. Since $\mathsf{Var}(\hat{\tau}_0)$ can be finite only for point-wise consistent estimators, this explains why we did not pursue asymptotic variance analysis of our timing and SAT estimators, which in practice will be only convergent to a set. This is not at all a shortcoming because, as we established analytically and tested with simulations, what matters in successful demodulation is energy capture.

Appendix B: Proof of Eq. (12)

Writing $n = kM + m$ with $m \in [0, M-1]$, we can re-express $r(t)$ in (3) as:

$$r(t) = \sqrt{\mathcal{E}} \sum_k s(kM) p_R(t - kMT_s - \tau_0) + \eta(t) + \rho(t)$$
$$+ \sqrt{\mathcal{E}} \sum_k \sum_{m=1}^{M-1} s(kM+m) p_R(t - (kM+m)T_s - \tau_0) \; ;$$

and its sample mean as [c.f. (5)]: $t \in [0, MT_s]$,

$$\bar{r}(t) = \frac{\sqrt{\mathcal{E}}}{N} \sum_{n=0}^{N-1} \sum_{k=n-1}^{n} s(kM) p_R(t + (n-k)MT_s - \tau_0) + \bar{\eta}(t) + \bar{\rho}(t)$$
$$+ \frac{\sqrt{\mathcal{E}}}{N} \sum_{m=1}^{M-1} \sum_{n=0}^{N-1} \sum_{k=n-2}^{n} s(kM+m) p_R(t + ((n-k)M - m)T_s - \tau_0) \; ,$$

where only two or three summands contribute in the sums over k, because we focus on a single period (notice that $t \in [0, MT_s]$). We next observe that for N sufficiently large, $\sum_{n=0}^{N-1} s((n-1)M) \doteq \sum_{n=0}^{N-1} s(nM) := N\bar{S}_0$; and likewise $\sum_{n=0}^{N-1} s((n-2)M+m) \doteq \sum_{n=0}^{N-1} s((n-1)M+m) \doteq \sum_{n=0}^{N-1} s(nM+m) := N\bar{S}_m$. Substituting the latter in the above expression of $\bar{r}(t)$ leads us to (12).

APPENDIX C: VARIANCE OF $\eta(k;\tilde{\tau}_0)$ IN (14)

Passing $\eta(t)$ through the matched filter with impulse response $p_R(-t+\hat{\tau}_0-\tau_0),\ t\in[-T_R,0]$, yields as output: $\zeta(t)=\int_0^{T_R} p_R(u+\hat{\tau}_0-\tau_0)\eta(t+u)du$. Since $\eta(t)$ is AWGN with double sided power spectral density $N_0/2$ and bandwidth W, which is assumed to be larger than the matched filter bandwidth, we deduce that $\zeta(t)$ is also Gaussian with power spectral density $(N_0/2)|H(f)|^2$. As $\eta(k;\tilde{\tau}_0)=\zeta(kT_s+\hat{\tau}_0)$, it follows readily that:

$$\begin{aligned}\mathsf{Var}(\eta(k;\tilde{\tau}_0)) &= (N_0/2)\int |H(f)|^2 df \\ &= (N_0/2)\int_0^{T_R} p_R^2(t-\tilde{\tau}_0)dt := E_C(\tilde{\tau}_0)N_0/2\ .\end{aligned}$$

REFERENCES

[1] J. C. Chen, K. Yao, and R. E. Hudson, "Source localization and beamforming," *IEEE Signal Processing Mag.*, vol. 19, no. 2, pp. 30-39, Mar. 2002.

[2] R. J.-M. Cramer, R. A. Scholtz, and M. Z. Win, "Evaluation of an ultra-wideband propagation channel," *IEEE Trans. Antennas and Propagation*, vol. 50, no. 5, pp. 561-570, May 2002.

[3] A. V. Dandawate and G. B. Giannakis, "Asymptotic theory of mixed time averages and kth-order cyclic moment and cumulant statistics," *IEEE Trans. Inform. Theory*, vol. 41, no. 1, pp. 216-232, Jan. 1995.

[4] G. B. Giannakis, "Filterbanks for blind channel identification and equalization," *IEEE Signal Processing Lett.*, vol. 4, pp. 184-187, June 1997.

[5] E. A. Homier and R. A. Scholtz, "Rapid acquisition of ultra-wideband signals in the dense multi-path channels," in *Proc. Conf. on Ultra-Wideband Systems and Technologies 2002*, pp. 105-110.

[6] IEEE P802.15 Working Group for WPANs, *Channel Modeling Sub-Committee Report Final*, IEEE P802.15-02/368r5-SG3a, Nov. 2002.

[7] IEEE P802.15 Working Group for WPANs, *Time Variance for UWB Wireless Channels*, IEEE P802.15-02/461r1-SG3a, Nov. 2002.

[8] J. N. Laneman and G. Wornell, "Distributed space-time coded protocols for exploiting cooperative diversity in wireless networks," *IEEE Trans. Inform. Theory*, vol. 49, pp. 2415-2425, Oct. 2003.

[9] V. Lottici, A. D. Andrea, and U. Mengali, "Channel estimation for ultra-wideband communications," *IEEE J. Select. Areas Commun.*, vol. 20, pp. 1638-1645, Dec. 2002.

[10] X. Luo and G. B. Giannakis, "Cyclic-mean based synchronization and efficient demodulation for UWB ad hoc access: generalizations and comparisons," *EURASIP Signal Processing*, 2006 (to appear). Downloadable from: http://spincom.ece.umn.edu/journal.html

[11] X. Luo, L. Yang, and G. B. Giannakis, "Designing optimal pulse-shapers for ultra-wideband radios," *J. Commun. and Networks*, vol. 5, no. 4, pp. 344-353, Dec. 2003.

[12] U. Mengali and A. D. Andrea, *Synchronization Techniques for Digital Receivers*. New York: Plenum Press, 1997.

[13] I. Oppermann, L. Stoica, A. Rabbachin, Z. Shelby, and J. Haapola, "UWB wireless sensor networks: UWEN: a practical example," *IEEE Commun. Mag.*, vol. 42, no. 12, pp. S27-S32, Dec. 2004.

[14] D. Porrat and D. Tse, "Bandwidth scaling in ultra wideband communication," in *Proc. 41st Allerton Conf.*, Oct. 2003.

[15] G. J. Pottie and W.J. Kaiser, "Wireless integrated network sensors," *Commun. of the ACM*, vol. 43, no. 5, pp. 551-8, May 2000.

[16] T. S. Rappaport, *Wireless Communications: Principles and Practice, 2nd Edition*. Prentice Hall, 2001.

[17] S. Roy, J. R. Foerster, V. S. Somayazulu, and D. G. Leeper, "Ultra-wideband radio design: the promise of high-speed, short-range wireless connectivity," *Proc. IEEE*, vol. 92, no. 2, pp. 295–311, Feb. 2004.

[18] A. Sendonaris, E. Erkip, and B. Aazhang, "User cooperation diversity: parts I and II," *IEEE Trans. Commun.*, vol. 51, no. 11, pp. 1927-1948, Nov. 2003.

[19] E. G. Strom, S. Parkvall, and S. L. Miller, "Propagation delay estimation in asynchronous direct-sequence code-division multiple access systems," *IEEE Trans. Commun.*, vol. 44, pp. 84-93, Jan. 1996.

[20] Z. Tian and G. B. Giannakis, "BER sensitivity to mis-timing in ultra-wideband communications, Part I/Part II: non-random channels/fading channels," *IEEE Trans. Signal Processing*, vol. 53, no. 4/5, pp. 1550-1560/1897-1907, April/May 2005.

[21] Z. Tian and G. B. Giannakis, "A GLRT approach to data-aided timing acquisition in UWB Radios, Part I/Part II," *IEEE Trans. Wireless Commun.*, vol. 4, no. 6, pp. 2956-2967/2994-3004, Nov. 2005.

[22] M. K. Tsatsanis and G. B. Giannakis, "Blind estimation of direct sequence spread spectrum signals in multipath," *IEEE Trans. Signal Processing*, vol. 45, pp. 1241-1252, May 1997.

[23] Z. Wang and G. B. Giannakis, "Wireless multicarrier communications: where Fourier meets Shannon," *IEEE Signal Processing Mag.*, vol. 17, no. 3, pp. 29-48, May 2000.

[24] Z. Wang and X. Yang, "Ultra wide-band communications with blind channel estimation based on first-order statistics," in *Proc. IEEE Intl. Conf. on ASSP 2004*.

[25] Z. Xu, "Asymptotically near-optimal blind estimation of multipath CDMA channels," *IEEE Trans. Signal Processing*, vol. 49, pp. 2003-2017, Sept. 2001.

[26] L. Yang and G. B. Giannakis, "Blind UWB timing with a dirty template," in *Proc. Intl. Conf. on ASSP 2004*; see also *Proc. GLOBECOM 2003*, pp. 769-773.

[27] L. Yang and G. B. Giannakis, "Ultra-wideband communications: an idea whose time has come," *IEEE Signal Processing Mag.*, vol. 21, no. 6, pp. 26-54, Nov. 2004.

[28] G. T. Zhou, M. Viberg, and T. McKelvey, "A first-order statistical method for channel estimation," *IEEE Signal Processing Lett.*, vol. 10, pp. 57-60, Mar. 2003.

[29] http://216.153.156.169:8080/rcd/rcdpdf/P1410-P2420.pdf

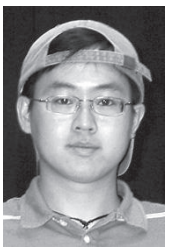

Xiliang Luo (S'03) received his B.S. degree in Physics from the Peking University, Beijing, China, in 2001, and M.Sc. degree in Electrical Engineering from the University of Minnesota, in 2003. He is currently a Ph.D. student in the Department of Electrical and Computer Engineering at the University of Minnesota. His general research interests lie in signal processing, communications, and information theory. Currently, he is focusing on ultra-wideband (UWB) communications and wireless sensor networks (WSN).

G. B. Giannakis (F'97) received his Diploma in Electrical Engineering from the National Technical University of Athens, Greece, 1981. From September 1982 to July 1986 he was with the University of Southern California (USC), where he received his MSc. in Electrical Engineering, 1983, MSc. in Mathematics, 1986, and Ph.D. in Electrical Engineering, 1986. After lecturing for one year at USC, he joined the University of Virginia in 1987, where he became a professor of Electrical Engineering in 1997. Since 1999 he has been a professor with the Department of Electrical and Computer Engineering at the University of Minnesota, where he now holds an ADC Chair in Wireless Telecommunications.

His general interests span the areas of communications and signal processing, estimation and detection theory, time-series analysis, and system identification – subjects on which he has published more than 200 journal papers, 350 conference papers and two edited books. Current research focuses on transmitter and receiver diversity techniques for single- and multi-user fading communication channels, complex-field and space-time coding, multicarrier, ultra-wide band wireless communication systems, cross-layer designs and sensor networks.

G. B. Giannakis is the (co-) recipient of six paper awards from the IEEE Signal Processing (SP) and Communications Societies (1992, 1998, 2000, 2001, 2003, 2004). He also received the SP Society's Technical Achievement Award in 2000. He served as Editor in Chief for the *IEEE SP Letters*, as Associate Editor for the *IEEE Trans. on Signal Proc.* and the *IEEE SP Letters*, as secretary of the SP Conference Board, as member of the SP Publications Board, as member and vice-chair of the Statistical Signal and Array Processing Technical Committee, as chair of the SP for Communications Technical Committee and as a member of the IEEE Fellows Election Committee. He has also served as a member of the IEEE-SP Society's Board of Governors, the Editorial Board for the *Proceedings of the IEEE* and the steering committee of the *IEEE Trans. on Wireless Communications*.